RSC Advances

PAPER

View Article Online
View Journal | View Issue

Open Access Article. Published on 13 December 2017. Downloaded on 11/5/2025 7:04:38 PM.
This article is licensed under a Creative Commons Attribution 3.0 Unported Licence.

Check for updates

Cite this: *RSC Adv.*, 2017, 7, 56183

Electrospun porous poly(tetrafluoroethylene-*co*-hexafluoropropylene-*co*-vinylidene fluoride) membranes for membrane distillation†

Yong Zhang,[abc] Bin Yang,[d] Kuiling Li,[abc] Deyin Hou,[abc] Changwei Zhao[abc] and Jun Wang*[abc]

A novel terpolymer (abbreviated as THV), which is a copolymer of tetrafluoroethylene, hexafluoropropylene, and vinylidene fluoride, that possesses advantages of excellent hydrophobicity, mechanical properties, and chemical resistance is an ideal material for membrane distillation. In this study, THV hydrophobic membranes were fabricated by the electrospinning method. Morphology and properties (pore size distribution, liquid entry pressure, porosity, and contact angle) of the THV electrospun membranes with various fabrication conditions (solvent composition, THV concentration, and applied voltage) were systematically studied. Under the optimized condition, the membrane exhibited a good structure, wetting resistance, and surface hydrophobicity. The mean pore size, liquid entry pressure of water (LEP_w), and contact angle were 0.79 μm, 118.0 kPa, and 130.7°, respectively. Owing to the advantages of the raw material and fabrication method, the membrane showed excellent mechanical properties and desalination performance. The tensile strength was 5.41 MPa, and the elongation at break was 247.9%, which were 2.47 and 5.61 times higher than those of the poly(vinylidene fluoride) (PVDF) membrane, respectively. Additionally, the membrane distillation flux was 4.42 kg m^{-2} h^{-1}, which was 1.93 times higher than that of the PVDF counterpart obtained under the same test condition *via* sweeping gas membrane distillation, and the salt rejection rate was higher than 99.8%.

Received 6th September 2017
Accepted 19th November 2017

DOI: 10.1039/c7ra09932k

rsc.li/rsc-advances

1 Introduction

Membrane distillation (MD) is a promising desalination technique owing to its unique merits such as extremely high salt rejection rate, low temperature, low pressure, and less sensitivity to fouling. Furthermore, MD is more attractive when coupled with solar energy or a low-grade heat source.[1,2] Although MD has a promising future, its commercialization has still been constrained due to various reasons at present. Moreover, one of the most important issues is the lack of a suitable membrane for this particular process.[3,4] During the last few years, significant attention has been paid to the membrane fabrication technique.[4–8] In addition, researchers have suggested that an ideal membrane should satisfy a series of requirements, which should cover not only structure properties (pore size distribution, bubble pore size, membrane thickness, porosity, and tortuosity) and thermal properties (thermal conductivity and stability) of the membrane, but also its surface hydrophobicity and mechanical properties.[3,9,10]

To date, polypropylene (PP), PVDF, and poly(tetrafluoroethylene) (PTFE) are widely employed because of their intrinsic hydrophobicity.[4] In addition, many novel polymers, including polystyrene,[11,12] polyazole,[13] as well as copolymer of PVDF and PTFE,[4,14–20] have been used to prepare membranes for MD to achieve better performance. Among them, the most promising material is the partially fluorinated copolymer of PVDF and PTFE. Poly(vinylidene fluoride-*co*-tetrafluoroethylene) (F2.4) has been employed for the preparation of flat sheet membranes for MD. This new kind of membrane exhibited a higher contact angle and water permeate flux as compared to the PVDF membrane.[21] Poly(vinylidene fluoride-*co*-chlorotrifluoroethylene) (PVDF-CTFE), another copolymer of PVDF, has also been used for membrane fabrication for MD. The result indicated that the membrane exhibited excellent membrane morphology, pore structure, and surface hydrophobicity. Moreover, the water flux was much higher than that of the PVDF membrane.[15] Poly(vinylidene fluoride-*co*-hexafluoropropylene) (PVDF-HFP) has also been studied, and this new type of membrane not only exhibits better

[a]*State Key Laboratory of Environmental Aquatic Chemistry, Research Center for Eco-Environmental Sciences, Chinese Academy of Sciences, 18 Shuangqing Road, Beijing 100085, China. E-mail: junwang@rcees.ac.cn; Tel: +86-10-62917207*

[b]*National Engineering Laboratory for Industrial Wastewater Treatment, Research Center for Eco-Environmental Sciences, Chinese Academy of Sciences, 18 Shuangqing Road, Beijing, 100085, China*

[c]*University of Chinese Academy of Sciences, 19 Yuquan Road, Beijing, 100049, China*

[d]*School of Chemical Engineering and Technology, Heibei University of Technology, 5340 Xiping Road, Tianjin, 300130, China*

† Electronic supplementary information (ESI) available. See DOI: 10.1039/c7ra09932k

Open Access Article. Published on 13 December 2017. Downloaded on 11/5/2025 7:04:38 PM.
This article is licensed under a Creative Commons Attribution 3.0 Unported Licence.

performance in terms of hydrophobicity and water permeability, but also reveals better mechanical properties.[16] In addition, Hyflon AD60 (a copolymer of TFE and 2,2,4-trifluoro-5-trifluoromethoxy-1,3-dioxole) has been used for hollow fiber membrane fabrication by a non-solvent-induced phase separation (NIPS) method. The water contact angle of the membrane was as high as 138° without any special treatment.[18] The abovementioned studies reveal that the raw material is crucial for the fabrication of membranes for MD.

Poly(TFE-*co*-HFP-*co*-VDF) (THV), a terpolymer of tetrafluoroethylene, hexafluoropropylene and vinylidene fluoride, possesses outstanding hydrophobicity, chemical resistance,[22–24] and mechanical properties[25] and appears to be another excellent fluorinated copolymer for membrane fabrication for MD. In previous studies, the fabrication of hydrophobic thin films through both NIPS and electrospinning methods has been investigated. The result indicated that the water contact angles of the films were as high as 118° and 145°.[22,23] However, the as-prepared films in these studies were not suitable for MD application due to lack of interconnected pores. To the best of our knowledge, except for the abovementioned two studies, no other studies have been reported on the THV membrane. According to the preliminary experiment, it is difficult for THV to form a porous membrane *via* the conventional NIPS method. This may be the main reason for the lack of research on the THV membrane.

Electrospinning is a versatile technique for the preparation of a nanofiber porous membrane. An electrospun membrane possesses high porosity and an interconnected open-pore structure. In addition, the membrane properties, such as pore size, porosity, and membrane thickness, can be easily tailored by adjusting the electrospinning parameters.[26–28] Therefore, electrospinning has become an attractive method for the fabrication of membranes including hydrophobic membranes for the MD applications.[29–31] Porous PVDF flat sheet membranes have been prepared using an electrospinning method.[29] The membranes showed excellent hydrophobicity and mechanical properties. The water permeate flux was also reported to be higher than that obtained for the membrane fabricated by conventional methods. Moreover, more than 100 other polymers have been successfully electrospun into nanofiber membranes.[27,28,30,32] Thus, electrospinning seems to be a promising technique for THV membrane fabrication.

In the present study, we prepared THV membranes by the electrospinning method. The effects of different electrospinning parameters (such as solvent composition, THV concentration, electrospinning time, and applied voltage) on the membrane morphology and properties were studied. To demonstrate the potential of the membrane for MD application, various characterization analyses have been carried out including scanning electron microscopy (SEM), contact angle measurement, pore size and porosity measurements, mechanical property test, LEP_w test, and so on. Then, the desalination performance was measured through sweeping gas membrane distillation. For comparison, a PVDF membrane has also been fabricated in this research.

2 Experimental

2.1 Materials

THV (221GZ, 3M Dyneon, USA) and PVDF (Solef 1010, Solvay, Belgium) resins were used for membrane fabrication. Acetone (AR, Sinopharm, China), dimethylformamide (DMF, AR, Sinopharm, China), and *N*,*N*-dimethylacetamide (DMAc, AR, Sinopharm, China) were employed as solvents. Other chemicals employed in this investigation were PTFE (5 μm, Aladdin, China), PVDF-HFP (Sigma-Aldrich, USA), FC 40 (3M Fluorinert, USA), and NaCl (AR, Sinopharm, China). All the abovementioned chemicals were used as received.

2.2 Membrane preparation

Both THV and PVDF membranes were prepared in this research. PVDF membranes prepared by the NIPS method are very popular; therefore, they have been chosen for comparison.

The THV and PVDF resins were dried at 60 °C for 24 h before preparation of a dope solution. Different amounts of solvent and polymer were mixed in sealed breakers and stirred at room temperature until homogeneous solutions were obtained. The details of the THV dope solution compositions can be found in Table 1. The PVDF dope solution consisted of 75 wt% DMAc, 20 wt% polymer, and 5 wt% acetone.[33] Then, the dope solutions were degassed in a vacuum oven at 60 °C for 30 min.

An electrospinning setup (TL-01, Tongli Ltd., China) was used for THV membrane preparation. It consisted of two plastic syringes (30 mL) connected to a two-channel injection pump (LSP02-1B, Longer Pump Ltd., China) for flow rate control, two metallic needles (inner diameter: 0.51 mm), a rotating drum collector, and high-voltage power supply. All membranes were fabricated onto polyester non-woven fabrics (thickness: 0.15 mm) using various electrospinning conditions (Table 1). Other conditions including the tip-to-collector distance, total feed flow rate, chamber temperature, and relative humidity were fixed at 10 cm, 2 mL h^{-1}, 55 °C, and 30%, respectively. After electrospinning, the membranes were dried at room temperature for 48 h to remove the residual solvent.

For PVDF membrane preparation, the dope solution was first cast on a glass plate with a knife. After being exposed to air at room temperature for 30 s, the film was immersed in a water bath for 24 h. After complete coagulation, the membrane was dried in air for another 24 h.[33]

2.3 Material, solution, and membrane characterization

Fourier-transform infrared (FT-IR) spectra (Nicolet 8700, Thermo Fisher Scientific, USA) were acquired to compare the THV, PVDF, PVDF-HFP, and PTFE polymer structures, as well as to monitor any residual solvent in the electrospun membrane. Membranes and raw materials were dried and fixed with a smart OMNI-sampler. Each spectrum was scanned for 64 times, and the resolution was 0.5 cm^{-1}.

The viscosities of the THV solutions with various polymer concentrations and solvent compositions were measured using a cone-and-plate viscometer (Cap 2000+, Brookfield, USA) with a no. 4 spindle. The rotating speed, operation temperature,

Open Access Article. Published on 13 December 2017. Downloaded on 11/5/2025 7:04:38 PM.
This article is licensed under a Creative Commons Attribution 3.0 Unported Licence.

Table 1 Dope solution compositions and electrospinning conditions of THV membranes

Membranes code	Solvents (%, wt/wt)		THV concentration (%, wt/wt)	Applied voltage (kV)	Spinning time (h)
	DMF	Acetone			
M1	**50**	**50**	15	15	12
M2	**60**	**40**	15	15	12
M3	**70**	**30**	15	15	12
M4	**80**	**20**	15	15	12
M5	**90**	**10**	15	15	12
M6	**100**	**0**	15	15	12
M7	100	0	**10**	15	12
M8	100	0	**20**	15	12
M9	100	0	15	**10**	12
M10	100	0	15	**20**	12
M11	100	0	15	**25**	12
M12	100	0	15	15	**20**
M13	100	0	15	15	**15**
M14	100	0	15	15	**9**
M15	100	0	15	15	**6**

running time, and holding time were 750 rpm, 55 °C, 12 s, and 1 s, respectively.

The morphology of the membrane surface was investigated through SEM (S-3000N, Hitachi Ltd., Japan). Membrane samples were first dried at 50 °C for 12 h and then fastened to an objective table with conducting resin. To improve the electrical conductivity, the samples were sputtered with platinum for 30 s before observation. The sputtering process was carried out using the Hitachi E-1000 ion sputtering device at a pressure lower than 10 Pa. The fiber diameters were measured from the SEM images using a software program (Nano Measurer, developed by Fudan University, China). For each sample, three SEM images were considered, and at least 200 fibers were measured.

The pore size was measured using a capillary flow porometer (Porolux 1000, Dataphysics, Germany). FC 40 was used as the wetting fluid, and the pore size was calculated from the gas flow rate and pressure based on the Young–Laplace equation. The porosity was measured by gravimetry, and FC 40 was employed as the wetting reagent. The membrane weights before and after wetting were measured using a high-sensitivity balance (0.1 mg resolution; AL104, Mettler Toledo, Switzerland). Porosity (ε) was obtained from the following equation:

$$\varepsilon = 1 - \frac{m_d/\rho_{THV}}{(m_w - m_d)/\rho_{FC\ 40} + m_d/\rho_{THV}} \quad (1)$$

where m_d, m_w, ρ_{THV}, and $\rho_{FC\ 40}$ are the dry membrane weight (kg), wetted membrane weight (kg), and densities of THV and FC 40 (kg m^{-3}), respectively. The THV and FC 40 densities are 1.81 and 1.85 × 10^3 kg m^{-3}, respectively. The membrane thickness was measured using the SEM images.

The contact angles were measured using an optical system (OCA15, Dataphysics, Germany) equipped with a charge-coupled device camera; 1 μL of distilled water was dropped on the membrane surface, and the image was obtained immediately.

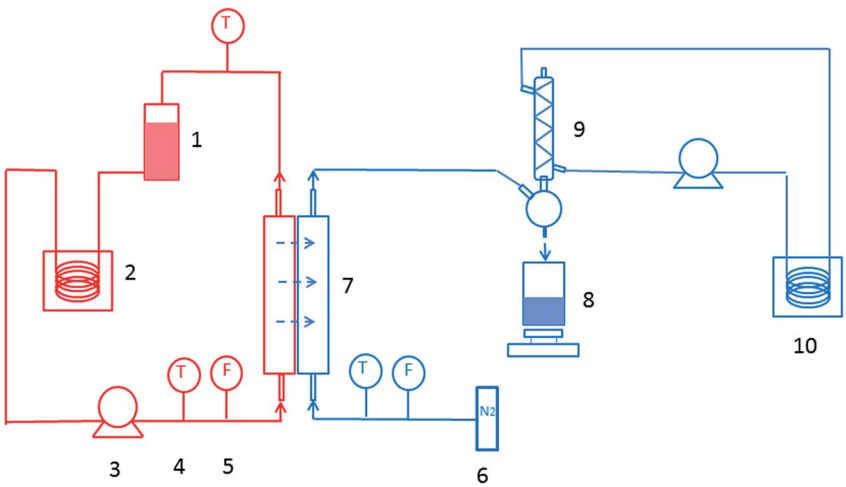

Fig. 1 Schematic of the sweeping gas membrane distillation process. (1) Feed reservoir; (2) heating bath; (3) feed pump; (4) thermometer; (5) flowmeter; (6) nitrogen cylinder; (7) membrane module; (8) permeate water tank and balance; (9) condenser; (10) cooling bath.

Open Access Article. Published on 13 December 2017. Downloaded on 11/5/2025 7:04:38 PM.
This article is licensed under a Creative Commons Attribution 3.0 Unported Licence.

Then, the contact angle was calculated using the image process software of the instrument. LEP_w has been measured using an experimental system described elsewhere,[34] which is the minimum applied pressure when water penetrates across the membrane.

Mechanical properties were investigated using an Instron tensiometer (5565-5kN, Instron Corporation, USA). The membrane samples were tailored to 80 mm in length and 30 mm in width. A constant elongation rate of 10 mm min^{-1} was employed at room temperature.

2.4 Sweeping gas membrane distillation experiments

The sweeping gas membrane distillation (SGMD) experiments were conducted using the experimental setup presented in Fig. 1. The membrane was placed in a poly methyl methacrylate module with an effective area of 3.05×10^{-3} m^2. Then, a 35 g L^{-1} NaCl solution was circulated as feed water by a peristaltic pump (BT300, Longer Pump Ltd., China), and the temperature was controlled by a heating bath (XMTD-2202, Yongshang Instruments, China). High-purity nitrogen (N_2 > 99.99%, water < 3×10^{-6}), provided by a cylinder, was employed as the sweeping gas, and the temperature was 18.0 ± 0.2 °C. A glass condenser connected to a cooling bath (SDC-6, Nanjing Xinchen Biotechnology, China) was used for the permeate water collection. The distillate water was obtained and measured every 20 min after the system was stabilized. The SGMD flux (J, kg m^{-2} h^{-1}) was calculated by the following equation:

$$J = \frac{m}{At} \tag{2}$$

where m is the quantity of distillate (kg), A is the membrane effective area (m^2), and t is the sampling time (h). The salt rejection ratio (R) was calculated using the following equation:

$$R = \frac{C_f - C_p}{C_f} \tag{3}$$

where C_f and C_p are the salt concentrations (mg L^{-1}) of the feed and distillate water, respectively.

3 Results and discussion

3.1 Properties of the polymers

THV is a terpolymer of TFE, HFP, and VDF. According to the chemical structure (presented in Fig. 2), it contains 59.4–76 wt% (59.4 wt% for PVDF, 76 wt% for PVDF-HFP and PTFE) fluorine that varies with the molar ratio of TFE, HFP, and VDF. The element content analysis showed that PVDF and THV contained 55.1 and 69.6 wt% fluorine, respectively. The result suggested that the THV membrane might be more hydrophobic with more fluorine than the PVDF membrane.

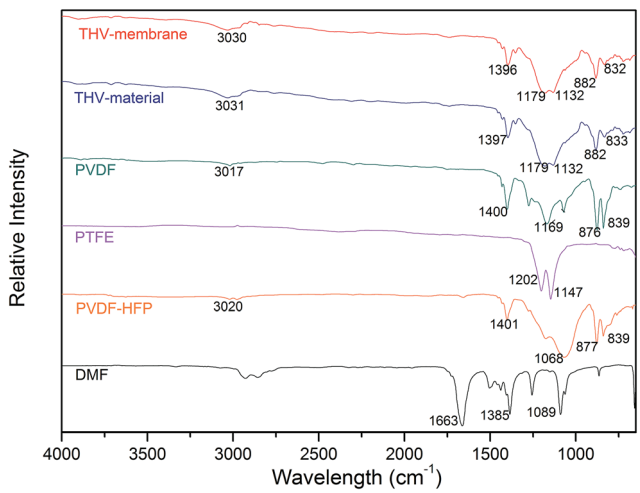

Fig. 3 FTIR spectra of THV (membrane and resin), PVDF, PTFE, PVDF-HFP, and DMF.

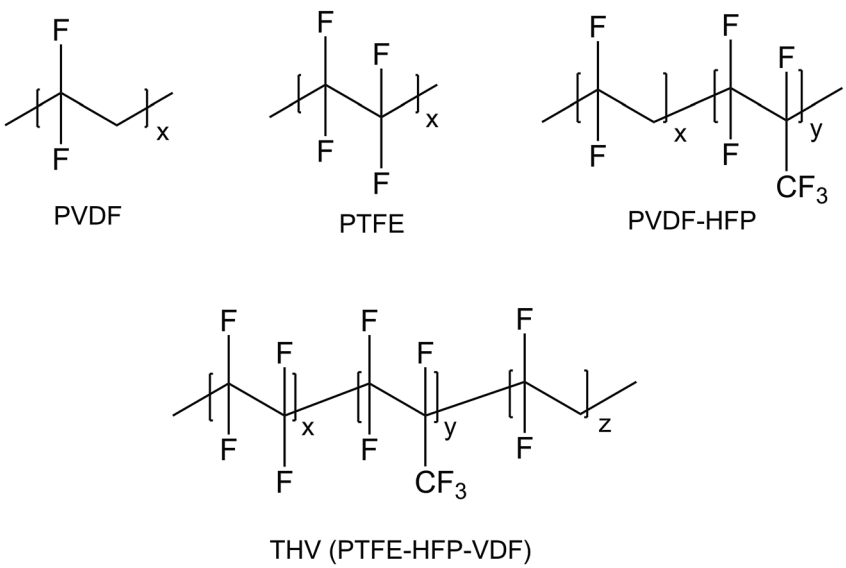

Fig. 2 Chemical structures of PVDF, PTFE, PVDF-HFP, and THV.

Open Access Article. Published on 13 December 2017. Downloaded on 11/5/2025 7:04:38 PM.
This article is licensed under a Creative Commons Attribution 3.0 Unported Licence.

The IR spectra of THV, PVDF, PTFE, and PVDF-HFP are shown in Fig. 3. PVDF exhibited distinct characteristic peaks assigned to $-CH_2$ bending (1400 cm^{-1}), $-CF_2$ stretching (1169 cm^{-1}), and amorphous phase absorption (876 and 839 cm^{-1}).[35] PTFE had characteristic peaks that were attributed to the $-CF_2$ asymmetrical (1202 cm^{-1}) and symmetrical (1147 cm^{-1}) stretching modes,[36] whereas PVDF-HFP showed a broad band at around 1068 cm^{-1}, assigned to the $-CF_2$ and $-CF_3$ stretching absorptions.[37] THV was expected to show all the characteristic peaks of these three polymers as it contained the three kinds of chain segments. Indeed, as presented in Fig. 3,

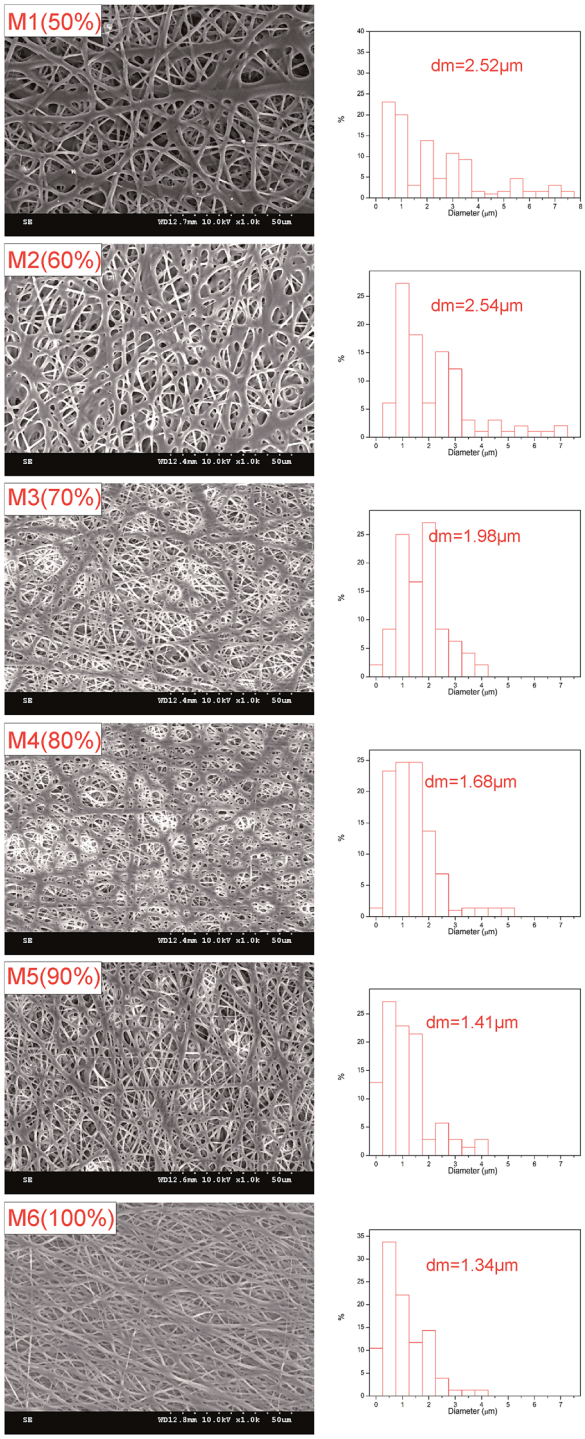

Fig. 4 Morphologies, fiber diameter distributions, and mean fiber diameters (d_m) of membranes prepared using different solvent compositions.

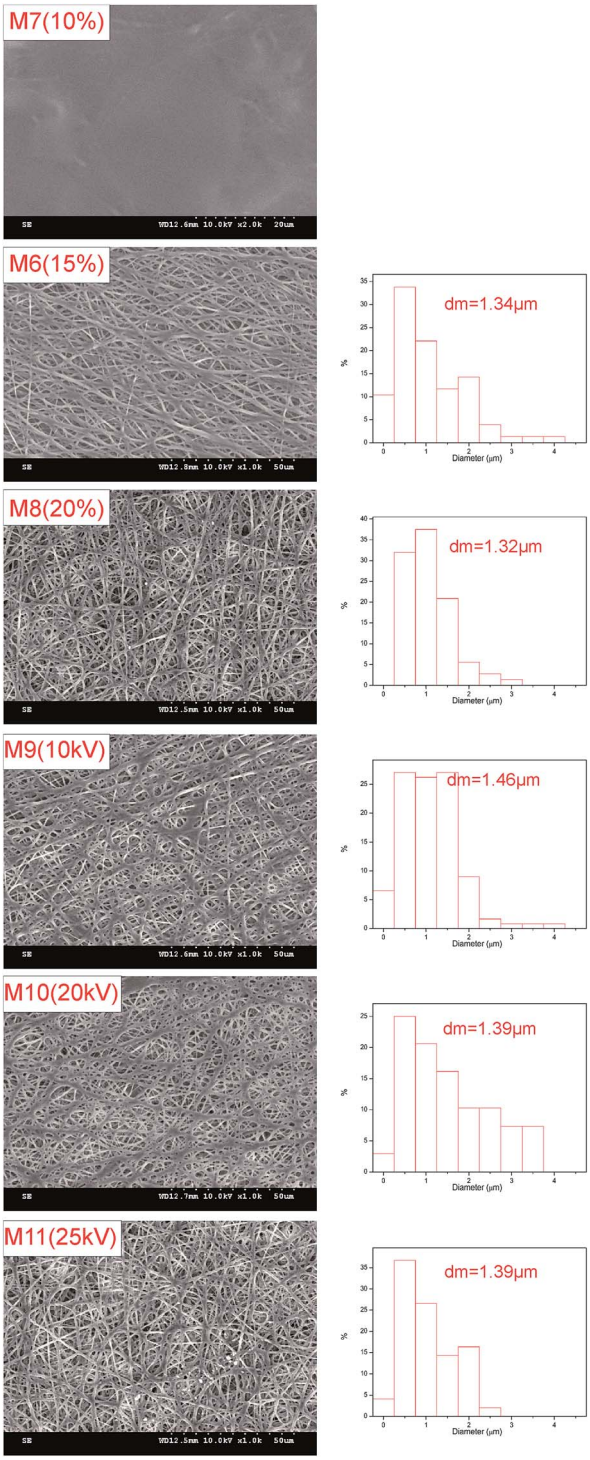

Fig. 5 Morphologies, mean fiber diameters (d_m), and fiber diameter distributions of membranes prepared from solutions with different THV concentrations (M6–M8) and at various applied voltages (M6, M9–M11).

Open Access Article. Published on 13 December 2017. Downloaded on 11/5/2025 7:04:38 PM.
This article is licensed under a Creative Commons Attribution 3.0 Unported Licence.

apart from the distinct peaks assigned to $-CH_2$ bending (1398 cm^{-1}) and amorphous phase absorptions (882 and 832 cm^{-1}), a broad band also appeared at around 1150 cm^{-1}, which was assigned to the emergence of $-CF_2$ stretching, $-CF_3$ stretching, $-CH_2$ wagging, *etc.*

Apart from the polymers, THV electrospun membrane and DMF were also analysed. The spectra of the THV electrospun membrane and raw material appeared identical, and no peaks at 1663, 1385, and 1089 cm^{-1} (characteristic peaks of DMF, assigned to C=O stretching, $-CH_3$ bending, and C–N stretching, respectively) were observed. The spectra suggested that no changes occurred during the electrospinning process, and no residual solvent was left in the membrane.

3.2 Membrane morphology

Acetone is an excellent solvent for THV according to preliminary experiments; therefore, it was employed for dope solution preparation first. However, it dripped from the spinning nozzle as the viscosity of the solution was very low (0.322 Pa s). Therefore, DMF, another good solvent, was added to the dope solution to adjust the viscosity. No drops were observed until the proportion of DMF was more than 50 wt% in the solvent. Thus, six membranes (from M1 to M6 in Table 1) fabricated from solutions with mixed solvent containing 50–100 wt% DMF were studied in this research.

Fig. 4 shows the typical surface morphologies and fiber diameter distributions of the membranes. The mean fiber diameter was rather large when the DMF content was 50–60 wt% (M1 and M2). As the DMF content increased, the fiber diameter decreased accordingly. It is shown in Fig. 4 that the mean fiber diameter decreases from 2.52 to 1.34 μm as the DMF content in the mixed solvent increases from 50 to 100 wt%. The viscosities were 0.414, 0.430, 0.438, 0.465, 0.481, and 0.490 Pa s for the dope solution with 50, 60, 70, 80, 90, and 100 wt% DMF in the solvent, respectively. When the viscosity is low, electrospray and electrospinning occur simultaneously; thus, a film consisting of fibers and droplets would appear according to the previous studies.[38–40] However, in this investigation, no droplets have been observed. As the solidification of THV was slow, the droplet may have appeared first, but became unstable and spread out on the membrane, especially when the viscosity was low (M1 and M2). Therefore, fibers with a large diameter appeared instead of droplets. As the viscosity increased (M3 and M4), less droplets formed, and the fiber diameter decreased. When the dope solution viscosity was high enough (M5 and M6), homogenous fibers formed, and the diameter was small.

Membranes prepared from dope solutions with 10, 15, and 20 wt% THV have also been studied, and the membrane morphologies are presented in Fig. 5. A dense surface (M7) appeared instead of a porous surface for the membrane prepared from the 10 wt% THV dope solution. However, porous membranes (M6 and M8) consisting of numerous fibers were observed when 15 and 20 wt% THV solutions were used. The viscosities were 0.246, 0.490, and 0.866 Pa s for 10, 15, and 20 wt% THV solutions, respectively. When the viscosity was low (10 wt% THV), electrospray was dominant, and the film consisting of droplets appeared. Since the solidification of THV is slow, this film may spread out on the membrane. Thus, a smooth dense film was formed. Literature also exhibited a similar result.[39] As the shear stress inside the needles elevated with an increase in viscosity of the polymer solution, the pressure on the syringes elevated accordingly. When the solution contained 20 wt% THV, the electrospinning process was hindered as the pressure was very high; this led to the deformation of plastic syringes. Therefore, 15 wt% THV was selected.

Voltages ranging from 10 to 25 kV were applied, and the SEM images of the corresponding samples are shown in Fig. 5. The membrane morphologies and fiber diameters (M6, M9–M11) were quite similar (from 1.34 to 1.46 μm). It revealed that the THV solution was not sensitive to voltage. Moreover, several THV solutions dripped when the voltage was equal to or lower than 10 kV; this damaged the membrane. In consideration of energy saving, a relative low voltage of 15 kV was selected.

Table 2 Membrane properties of THV electrospun membranes with various dope compositions and electrospinning conditions

Membrane code	Thickness (μm)	Mean pore size (μm)	Maximum pore size (μm)	Porosity (%)	LEP_w (kPa)	Contact angle (°)	Fiber diameter (μm)
M1	106.7 ± 3.3	1.24 ± 0.09	1.81 ± 0.12	42.1 ± 3.2	84.4 ± 4.2	131.4 ± 1.0	2.52 ± 0.64
M2	117.0 ± 6.8	1.29 ± 0.08	1.73 ± 0.07	44.2 ± 7.6	86.7 ± 12.0	128.4 ± 3.8	2.54 ± 0.55
M3	123.1 ± 15.1	1.27 ± 0.02	1.72 ± 0.20	42.5 ± 7.4	82.7 ± 7.3	127.7 ± 1.4	1.98 ± 0.68
M4	159.1 ± 10.5	1.28 ± 0.08	1.85 ± 0.29	51.2 ± 7.8	95.4 ± 10.7	126.6 ± 3.0	1.68 ± 0.63
M5	169.3 ± 8.4	1.07 ± 0.01	1.41 ± 0.13	56.8 ± 2.5	101.4 ± 17.7	128.4 ± 1.6	1.41 ± 0.52
M6	153.9 ± 6.8	0.79 ± 0.02	1.05 ± 0.08	55.6 ± 4.3	118.0 ± 25.4	130.7 ± 1.9	1.34 ± 0.51
M7	25.0 ± 1.4	—		—	—	110.9 ± 0.6	—
M8	184.1 ± 11.2	0.75 ± 0.10	1.12 ± 0.03	57.7 ± 5.7	115.0 ± 4.2	126.9 ± 1.0	1.32 ± 0.41
M9	157.7 ± 4.5	0.83 ± 0.03	1.11 ± 0.12	54.2 ± 4.8	114.5 ± 4.9	127.0 ± 5.8	1.46 ± 0.52
M10	162.2 ± 10.3	0.80 ± 0.12	1.29 ± 0.20	55.0 ± 1.0	104.9 ± 24.1	125.6 ± 2.8	1.39 ± 0.61
M11	160.0 ± 10.7	0.80 ± 0.03	1.21 ± 0.15	53.3 ± 1.5	117.0 ± 7.1	127.2 ± 5.5	1.39 ± 0.55
M12	261.1 ± 10.1	0.84 ± 0.05	1.09 ± 0.07	51.8 ± 6.0	116.7 ± 3.5	131.3 ± 2.7	1.40 ± 0.57
M13	196.8 ± 10.0	0.88 ± 0.01	1.21 ± 0.11	53.4 ± 7.5	91.5 ± 1.0	127.0 ± 7.5	1.45 ± 0.64
M14	105.4 ± 5.1	0.83 ± 0.01	1.20 ± 0.17	55.3 ± 4.9	92.9 ± 10.1	126.8 ± 1.1	1.41 ± 0.41
M15	55.4 ± 7.0	0.83 ± 0.03	1.12 ± 0.02	53.5 ± 6.7	106.0 ± 1.4	128.8 ± 2.4	1.31 ± 0.44

Open Access Article. Published on 13 December 2017. Downloaded on 11/5/2025 7:04:38 PM.
This article is licensed under a Creative Commons Attribution 3.0 Unported Licence.

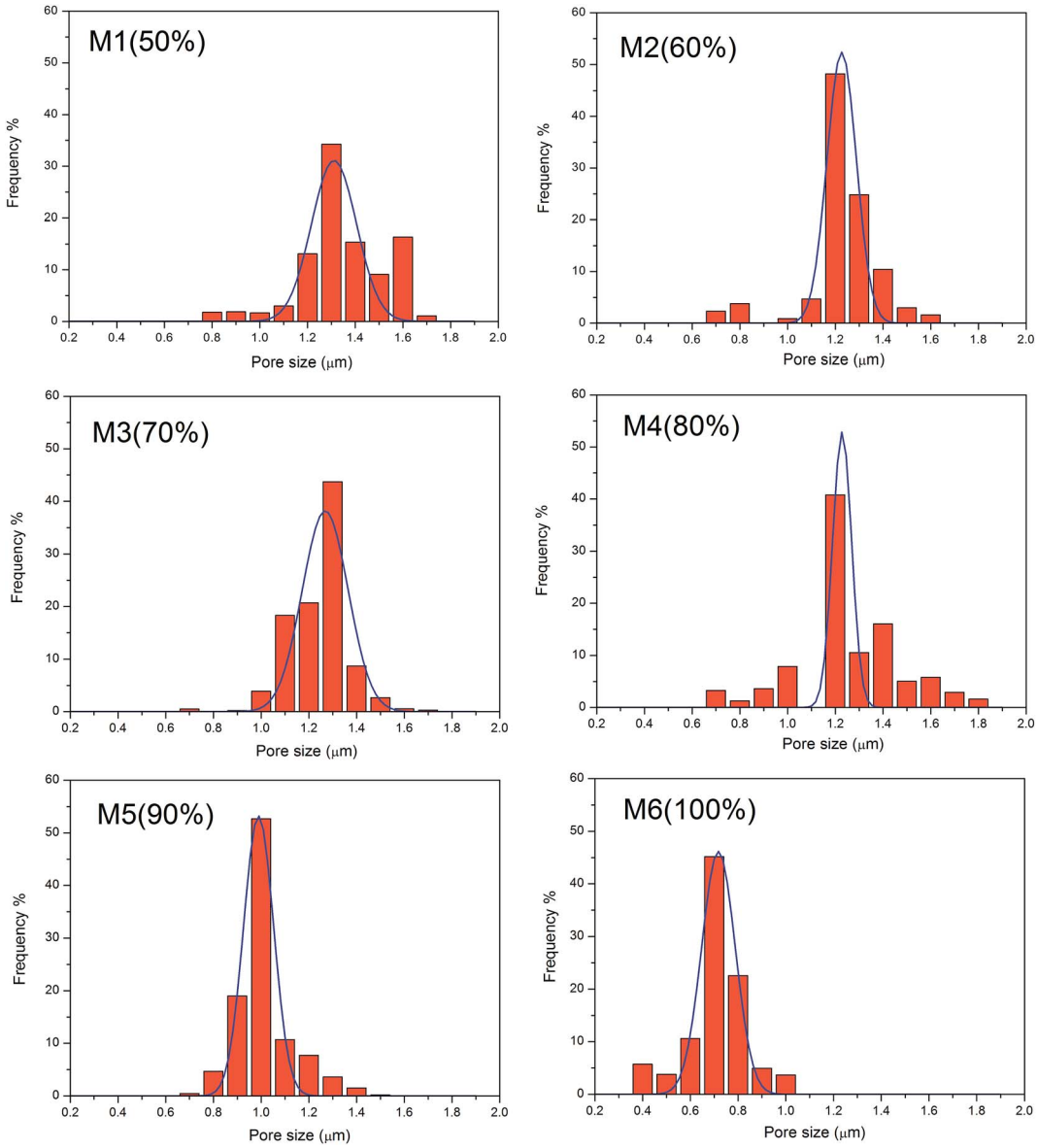

Fig. 6 Pore size distributions of the membranes prepared using different solvent compositions.

3.3 Pore size

It can be observed from Table 2 and Fig. 6 that the pore size is highly related to the fiber diameter. As the DMF content in the mixed solvent increased from 50 to 100 wt% (M1 to M6), the mean fiber diameter decreased from 2.52 to 1.34 μm. Accordingly, the mean pore size decreased from 1.24 to 0.79 μm. It can also be observed from the SEM images (Fig. 4) that the distance between fibers (related to pore size) decreases as the fiber density increases. Apart from the mean pore size, the maximum pore size also decreased from 1.81 to 1.05 μm as the DMF content increased from 50% to 100%. The THV concentration (15 wt% and 20 wt%) and applied voltage did not have much influence on the fiber diameter; thus, the pore size was maintained around 0.75–0.83 μm. According to previous studies, the pore size was recommended to be between 0.1 and 1 μm for high MD performance and good wetting resistance.[3,9,41] Thus, M6, with a mean pore size of 0.79 μm, was a good candidate for MD applications.

3.4 Wetting resistance and surface hydrophobicity

The wetting resistance is defined by LEP_w, which can be estimated from the following equation:[42]

$$LEP_w = \frac{-2B\gamma \cos\theta}{r_{max}} \quad (4)$$

where B is the geometric pore coefficient (in this research, cylindrical pores have been speculated and B equals to 1), γ is the water surface tension (N m^{-1}), θ is the contact angle (°), and r_{max} is the maximum pore size (m). The hydrophobicity (contact angle in Table 2) did not change much upon changing the dope solution compositions and fabrication conditions, which ranged from 125.6° to 131.4°. Thus, the LEP_w depended on the

Open Access Article. Published on 13 December 2017. Downloaded on 11/5/2025 7:04:38 PM.
This article is licensed under a Creative Commons Attribution 3.0 Unported Licence.

maximum pore size in this research. When the DMF content in the mixed solvent increased from 50 to 100 wt% (M1 to M6), the maximum pore size decreased from 1.81 to 1.05 μm, and the LEP_w increased from 84.4 to 118.0 kPa, respectively (presented in Table 2). The LEP_w of the electrospun THV membranes satisfies the requirement of MD application according to the literature.[29]

It can be observed from Fig. 7 that the contact angle for M7 (110.9°, 10 wt% THV) is much lower than that of M6 (130.7°, 15 wt% THV) and M8 (126.9°, 20 wt% THV). Although the membranes were fabricated from the same polymer, the surface hydrophobicity varied widely. As presented in Fig. 5, M7 had a smooth surface, whereas the others had a rough surface. The average surface roughness (R_a) of the membranes was 571 nm, 1094 nm, and 1048 nm for M7, M6, and M8, respectively (presented in Fig. S1†). When the membrane surface was rough, some air was trapped between the solid membrane and water. Thus, the area between solid and air increased, and the hydrophobicity elevated accordingly.[43–45] The PVDF membrane (prepared from the NIPS method) showed a contact angle of 91.9° (presented in Fig. 7), which was much lower than that of the THV membrane. The fluorine content of PVDF (55.1 wt%) was less than that of THV (69.6 wt%). In addition, the roughness was smaller (Fig. S1†). In conclusion, the high water contact angle of the THV membrane was attributed to the low surface energy material and rough surface structure.

3.5 Mechanical properties

Although MD always operates at relatively low pressures, membrane rupture may still occur due to hydraulic impact and flow disturbance for industrial applications;[29] thus, the membranes should possess good mechanical properties.

THV electrospun membranes (with different thicknesses) and the PVDF membrane (prepared from the NIPS method) were tested for mechanical properties. The stress–strain curves are shown in Fig. 8, and the mechanical property data are reported in Table 3. When the membrane thickness increased from 55.4 to 261.1 μm (by increasing the spinning time), the maximum loading increased from 3.20 to 15.57 N, respectively. The tensile strength was between 5.38 and 5.71 MPa, which indicated the homogeneous structure of the membrane. For comparison, the tensile strength was 2.19 MPa for the PVDF membrane. Moreover, the elongations at break ranged from 247.9% to 312.7% for the THV membranes, which was also higher than that of the PVDF membrane (44.2%). The THV resin has a higher elongation at break (700%) than PVDF (400%).[25] In addition, plenty of fibers in the THV membrane fused together, as shown in Fig. 4 and 5. Thus, the THV electrospun membranes showed better mechanical properties.

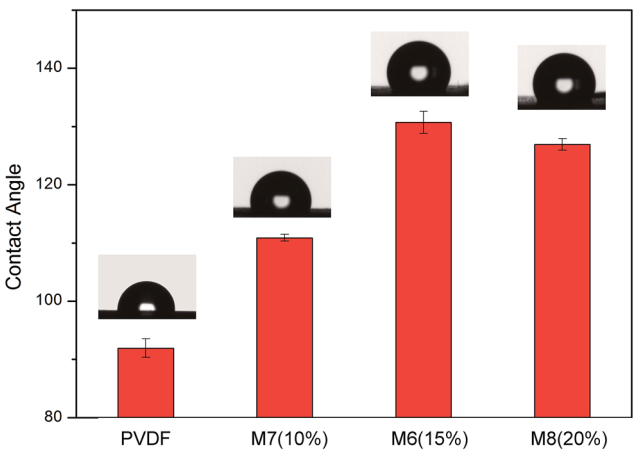

Fig. 7 Water contact angles for PVDF and THV electrospun membranes.

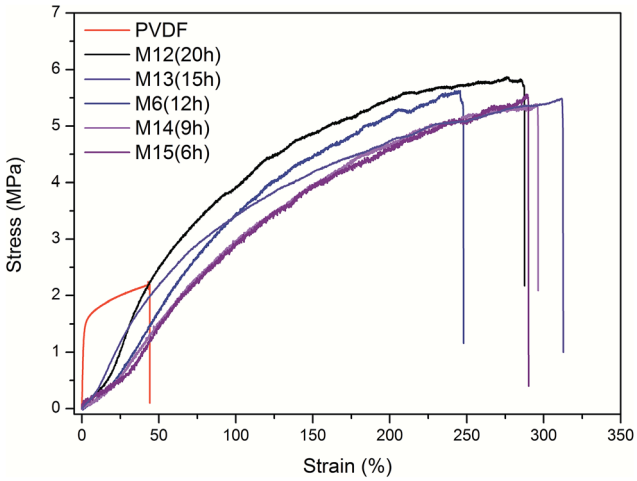

Fig. 8 Stress–strain curves of the PVDF membrane and the THV membranes prepared with different electrospinning times.

3.6 Membrane distillation performance

SGMD is relatively less studied because of the complicated system; however, it has a great perspective as it exhibits the advantages of a relatively low conductive heat loss and a reduced mass transfer resistance.[46] It was reported that 1.4 times higher flux and lower internal heat loss were obtained using SGMD as compared to the case of direct contact membrane distillation (DCMD) under the same feed condition.[47] Therefore, in this study, SGMD configuration was employed for desalination test.

As shown in Fig. 9, the flux increased with an increase in feed temperature. For the SGMD process, the water vapour permeate flux is a function of the transmembrane pressure difference

Table 3 Mechanical properties of the PVDF and THV membranes

Membrane	Tensile strength (MPa)	Elongation at break (%)	Young's module (MPa)
PVDF	2.19	44.2	14.23
M12 (20 h)	5.71	287.4	4.57
M13 (15 h)	5.48	312.7	4.69
M6 (9 h)	5.41	247.9	4.22
M14 (6 h)	5.38	296.3	3.13
M15 (3 h)	5.58	289.9	3.66

 This journal is © The Royal Society of Chemistry 2017

Open Access Article. Published on 13 December 2017. Downloaded on 11/5/2025 7:04:38 PM.
This article is licensed under a Creative Commons Attribution 3.0 Unported Licence.

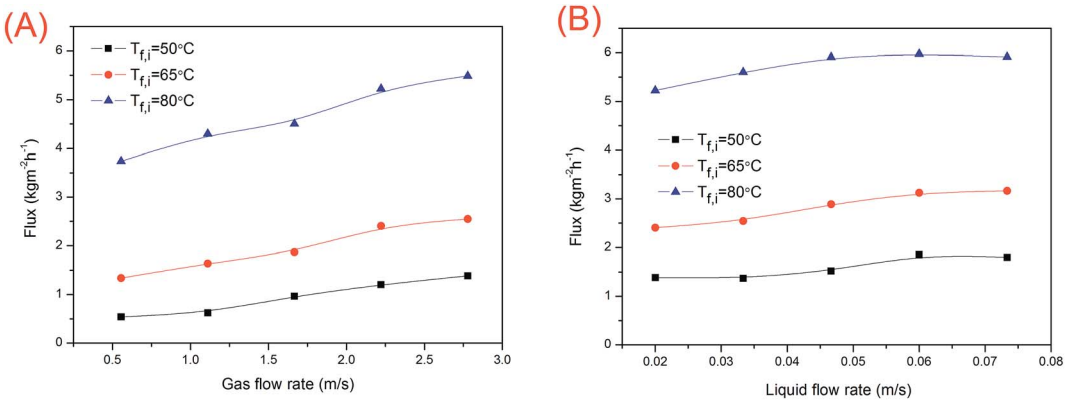

Fig. 9 (A) Effects of the gas flow rate and inlet feed water temperature on membrane distillation flux; (B) effects of the liquid flow rate and inlet feed water temperature on membrane distillation flux. M6 (electrospinning time: 12 h) was used.

between the feed water and the sweeping gas. In addition, the water vapour pressure increased exponentially with the increasing feed water temperature. As a result, the flux increased by 3.28–6.91 times when the feed water temperature increased from 50 to 80 °C (Fig. 9).

The temperature polarization of the permeate side reduced with an increase in the sweeping gas flow rate. Thus, the driving force increased. As shown in Fig. 9A, the water flux increased with an increase in the sweeping gas flow rate. The water flux was also promoted by the feed flow rate (Fig. 9B) due to the reduction in temperature and concentration polarizations in water. However, for SGMD, the total temperature polarization is governed by the sweeping gas side.[48] The effect of the temperature polarization reduction in water is less important. Thus, the flux was not affected markedly by the water flow rate.

The membrane distillation performances of THV electrospun membranes and PVDF membrane fabricated from the NIPS method were compared. The water permeate fluxes and salt rejection rates are shown in Fig. 10A. For THV membranes, the fluxes varied with the membrane thickness markedly. By reducing the membrane thickness, the mass transfer resistance decreases and the flux increases. M15 with a membrane thickness of 55.4 ± 7.0 μm showed the best membrane distillation performance with a flux of 7.38 kg m^{-2} h^{-1}. According to the literature, the mass flux can be expressed as follows:[3]

$$N \propto \frac{\Delta p}{\delta} \tag{5}$$

where Δp is the water interfacial vapour pressure (Pa) difference over the membrane, namely, driving force, and δ is the membrane thickness (m). However, the heat loss increased with a decrease in membrane thickness. Thus, the temperature polarization increased and the driving force decreased.[32] As shown in Fig. 10B, the rate of increase in flux slowed down when the membrane thickness parameter ($1/\delta$, μm^{-1}) increased. In addition, all the THV membranes showed great salt rejection rate higher than 99.8% (exhibited in Fig. 10A).

The PVDF membrane (thickness: 145.4 μm; mean pore size: 0.11 μm; water contact angle: 91.9°; and porosity: 75.8%) fabricated from the NIPS method was also tested *via* SGMD, and the flux was 2.28 kg m^{-2} h^{-1}. The THV electrospun membrane with a similar thickness (153.9 μm, M6) showed a flux of 4.42 kg m^{-2} h^{-1}, which was 1.93 times higher than that of the PVDF membrane. Although the porosity of the PVDF membrane (75.8%) was much higher than that of the THV membrane (55.6%), the THV membrane showed a better interconnected

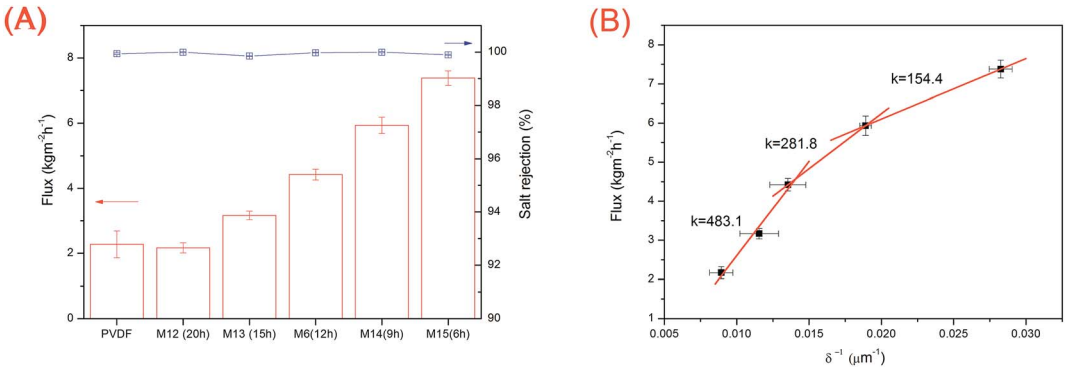

Fig. 10 (A) Membrane distillation flux and salt rejection rate for PVDF and THV membranes with various electrospinning times. (B) Relationship between membrane thickness and membrane distillation flux. For the abovementioned experiments, the inlet temperature of the feed solution (35 g L^{-1} NaCl) was 75 °C, whereas the flow rates of the gas and feed solution were 2.22 and 0.02 m s^{-1}, respectively.

Open Access Article. Published on 13 December 2017. Downloaded on 11/5/2025 7:04:38 PM. This article is licensed under a Creative Commons Attribution 3.0 Unported Licence.

pore structure with less blind pores (membrane cross sections were exhibited in Fig. S2†), and the tortuosity was smaller. As a result, the mass transfer resistance was smaller, and the flux was higher than that of the PVDF membrane.

4 Conclusions

In this study, THV membranes were fabricated *via* the electrospinning technique. The effects of solvent composition, THV concentration, and applied voltage on the membrane properties were investigated. The fiber diameter and pore size decreased with an increase in DMF content in the solvent. In addition, the wetting resistance (LEP_w) increased. The THV content also deeply affects the membrane fabrication. On the one hand, electrospun fiber formation was hindered with low THV content; on the other hand, the shear stress inside the needles was too high to spin with a high THV content. However, the applied voltage did not affect the membrane properties obviously. By comparing the membrane surface morphology, fiber diameter, pore size distribution, LEP_w, porosity, *etc.*, the optimized membrane fabrication conditions were chosen as follows: 100% DMF as a solvent, 15 wt% polymer, and 15 kV applied voltage. Moreover, the membrane possessed an interconnected pore structure, a suitable pore size, good wetting resistance, and hydrophobicity. The THV electrospun membrane also exhibited outstanding mechanical properties because of both the intrinsic property of the raw material and the membrane structure. The tensile strength and elongation at break (M6) were 5.41 MPa and 247.9%, respectively, which were much higher than those of the PVDF membrane (2.19 MPa for tensile strength and 44.2% for elongation at break). Due to the high interconnected pore structure with less blind pores, the THV electrospun membrane showed a flux that was 1.93 times higher than that of the PVDF membrane with a similar membrane thickness. The membrane distillation flux increased with a decrease in membrane thickness. M15 (membrane thickness: 55.4 ± 7.0 μm) showed the best membrane distillation performance with a flux of 7.38 kg m^{-2} h^{-1} and salt rejection rate higher than 99.8%. The electrospun THV membrane in this research revealed good membrane distillation performance.

Conflicts of interest

There are no conflicts to declare.

Acknowledgements

This research was financially supported by the National Key Research and Development Program of China (No. 2016YFC0400501) and the National Natural Science Foundation of China (No. 51578533).

References

1 S. Al-Obaidani, E. Curcio, F. Macedonio, G. Di Profio, H. Ai-Hinai and E. Drioli, *J. Membr. Sci.*, 2008, **323**, 85–98.
2 M. Khayet and T. Matsuura, in *Membrane Distillation*, Elsevier, Amsterdam, 2011, pp. 427–452.
3 L. Eykens, K. De Sitter, C. Dotremont, L. Pinoy and B. Van der Bruggen, *Ind. Eng. Chem. Res.*, 2016, **55**, 9333–9343.
4 P. Wang and T. S. Chung, *J. Membr. Sci.*, 2015, **474**, 39–56.
5 D. Y. Hou, H. Fan, Q. L. Jiang, J. Wang and X. H. Zhang, *Sep. Purif. Technol.*, 2014, **135**, 211–222.
6 H. L. Zhu, H. J. Wang, F. Wang, Y. H. Guo, H. P. Zhang and J. Y. Chen, *J. Membr. Sci.*, 2013, **446**, 145–153.
7 L. Eykens, K. De Sitter, C. Dotremont, L. Pinoy and B. Van der Bruggen, *Sep. Purif. Technol.*, 2017, **182**, 36–51.
8 L. X. Liu, F. Shen, B. W. Zhang, H. Q. Jiang, J. Y. Li, J. Q. Luo, H. H. Wu, R. Khan and Y. H. Wan, *RSC Adv.*, 2016, **6**, 107840–107850.
9 M. S. El-Bourawi, Z. Ding, R. Ma and M. Khayet, *J. Membr. Sci.*, 2006, **285**, 4–29.
10 M. Khayet, *Adv. Colloid Interface Sci.*, 2011, **164**, 56–88.
11 X. Li, C. Wang, Y. Yang, X. F. Wang, M. F. Zhu and B. S. Hsiao, *ACS Appl. Mater. Interfaces*, 2014, **6**, 2431–2438.
12 H. Ke, E. Feldman, P. Guzman, J. Cole, Q. Wei, B. Chu, A. Alkhudhiri, R. Alrasheed and B. S. Hsiao, *J. Membr. Sci.*, 2016, **515**, 86–97.
13 H. Maab, L. Francis, A. Al-Saadi, C. Aubry, N. Ghaffour, G. Amy and S. P. Nunes, *J. Membr. Sci.*, 2012, **423**, 11–19.
14 Z. Cui, E. Drioli and Y. M. Lee, *Prog. Polym. Sci.*, 2014, **39**, 164–198.
15 J. Wang, L. B. Zheng, Z. J. Wu, Y. Zhang and X. H. Zhang, *J. Membr. Sci.*, 2016, **497**, 183–193.
16 L. Shi, R. Wang, Y. Cao, C. Feng, D. T. Liang and J. H. Tay, *J. Membr. Sci.*, 2007, **305**, 215–225.
17 C. Feng, B. Shi, G. Li and Y. Wu, *Sep. Purif. Technol.*, 2004, **39**, 221–228.
18 D. Tong, X. Wang, M. Ali, C. Q. Lan, Y. Wang, E. Drioli, Z. Wang and Z. Cui, *Sep. Purif. Technol.*, 2016, **157**, 1–8.
19 Q. F. Alsalhy, K. T. Rashid, S. S. Ibrahim, A. H. Ghanim, B. Van der Bruggen, P. Luis and M. Zablouk, *J. Appl. Polym. Sci.*, 2013, **129**, 3304–3313.
20 L. B. Zheng, J. Wang, Y. S. Wei, Y. Zhang, K. Li and Z. J. Wu, *RSC Adv.*, 2016, **6**, 20926–20937.
21 C. S. Feng, B. L. Shi, G. M. Li and Y. L. Wu, *J. Membr. Sci.*, 2004, **237**, 15–24.
22 S. Ok, S. Sadaf and L. Walder, *High Perform. Polym.*, 2014, **26**, 779–789.
23 S. Ok, S. A. Furquan, Z. Khan and A. U. Dogan, *High Perform. Polym.*, 2016, **28**, 206–214.
24 H. Freimuth, C. Sinn and M. Dettenamaier, *Polymer*, 1996, **37**, 831–836.
25 3M™ Dyneon™ Fluoroplastic Granules THV 221GZ, http://www.3m.com/3M/en_US/company-us/search/~/3M-Dyneon-Fluoroplastic-Granules-THV-221GZ?N=5002385+3292678506&rt=rud.
26 C. Feng, K. C. Khulbe, T. Matsuura, S. Tabe and A. F. Ismail, *Sep. Purif. Technol.*, 2013, **102**, 118–135.
27 L. D. Tijing, J. S. Choi, S. Lee, S. H. Kim and H. K. Shon, *J. Membr. Sci.*, 2014, **453**, 435–462.
28 F. E. Ahmed, B. S. Lalia and R. Hashaikeh, *Desalination*, 2015, **356**, 15–30.

Open Access Article. Published on 13 December 2017. Downloaded on 11/5/2025 7:04:38 PM.
This article is licensed under a Creative Commons Attribution 3.0 Unported Licence.

29 M. Essalhi and M. Khayet, *J. Membr. Sci.*, 2013, **433**, 167–179.
30 Y. Liao, R. Wang, M. Tian, C. Q. Qiu and A. G. Fane, *J. Membr. Sci.*, 2013, **425**, 30–39.
31 H. Y. Wu, R. Wang and R. W. Field, *J. Membr. Sci.*, 2014, **470**, 257–265.
32 S. S. Ray, S. S. Chen, C. W. Li, N. C. Nguyen and H. T. Nguyen, *RSC Adv.*, 2016, **6**, 85495–85514.
33 D. Hou, G. Dai, J. Wang, H. Fan, L. Zhang and Z. Luan, *Sep. Purif. Technol.*, 2012, **101**, 1–10.
34 M. Essalhi and M. Khayet, *J. Membr. Sci.*, 2014, **454**, 133–143.
35 Y. Peng and P. Wu, *Polymer*, 2004, **45**, 5295–5299.
36 J. Su, G. Wu, Y. Liu and H. Zeng, *J. Fluorine Chem.*, 2006, **127**, 91–96.
37 R. A. Senthil, J. Theerthagiri, J. Madhavan, K. Murugan, P. Arunachalam and A. K. Arof, *J. Solid State Chem.*, 2016, **242**, 199–206.
38 Z. Li and C. Wang, *One-Dimensional Nanostructures*, Springer, Heidelberg, 2013.
39 L. M. M. Costa, R. E. S. Bretas and R. Gregorio, *Mater. Sci. Appl.*, 2010, **01**, 247–252.
40 J. M. Deitzel, J. Kleinmeyer, D. Harris and N. C. Beck Tan, *Polymer*, 2001, **42**, 261–272.
41 K. W. Lawson and D. R. Lloyd, *J. Membr. Sci.*, 1997, **124**, 1–25.
42 A. C. M. Franken, J. A. M. Nolten, M. H. V. Mulder, D. Bargeman and C. A. Smolders, *J. Membr. Sci.*, 1987, **33**, 315–328.
43 S. Yang, L. Chen, C. Wang, M. Rana and P.-C. Ma, *J. Colloid Interface Sci.*, 2017, **508**, 254–262.
44 S. Munirasu, F. Banat, A. A. Durrani and M. A. Haija, *Desalination*, 2017, **417**, 77–86.
45 X. J. Feng and L. Jiang, *Adv. Mater.*, 2006, **18**, 3063–3078.
46 M. Khayet and T. Matsuura, in *Membrane Distillation*, Elsevier, Amsterdam, 2011, pp. 295–322.
47 M. Khayet, M. P. Godino and J. I. Mengual, *Int. J. Nucl. Desalin.*, 2003, **1**, 30–47.
48 M. Khayet, M. P. Godino and J. I. Mengual, *AIChE J.*, 2002, **48**, 1488–1497.